A Method for Designing Stealth Radar Waveform and its Performance Analysis

Qiongdan Huang, Honggang Wang, Hanlu Zhang and JinWei Song

***Abstract*—In this study, the chaotic binary codes generated by quantum logistic map were adopted to modulate the phase of the orthogonal frequency division multiplexing (OFDM) signal, thus further designing a multicarrier chaotic phase coded radar waveform. Both the ambiguity function and the expression of the pulse compression of this waveform were deduced. In addition, pulse compression is performed on the signal using the segmented fast Fourier transform (FFT) method, which is compared with conventional pulse compression method accordingly. Simulation results suggest that by introducing multicarrier and chaotic phase modulation, the waveform can be improved in terms of complexity, randomness and coding agility. The signal designed in this study exhibits its easy accessibility in terms of signal receiving and processing due to the adopted FFT method, which is proven to be an effective low probability of interception (LPI) stealth radar waveform.**

***Index Terms*—multicarrier, chaos, radar signal, pulse compression**

I. Introduction

PERFORMING as one of the prioritized duties in realizing low probability of interception (LPI) technology and radio-frequency (RF) stealth, the philosophy of designing radar waveform takes into consideration studying or choosing certain waveforms to achieve stealth, to which the requirement for radar echo involves carrying target information while preventing from being intercepted, as well as minimizing possibilities of being attacked by precision guided weapons or anti-radiation missiles.

In order to realize stealth for radar waveforms, certain properties ought to be prioritized *ab initio* [1], of which include but not limited to maximum signal uncertainty, waveform complexity, coding agility, instantaneous bandwidth with wideness and uniformity, thumbtack-shaped ambiguity, large compression ratio, low sidelobe level, etc.

Manuscript received November 30, 2019; revised February 09, 2020. This research is sponsored by ‘Key Research and Development Program of Shaanxi Province with grant number 2018GY-150, 2018ZDXM-GY-041’, ‘Xi’an Science, Technology Plan Project, grant number 201805040YD18CG24-3’, The Natural Science Foundation of Education Department of Shaanxi Province, grant number 18JK0704.

Qiongdan Huang is with School of Communication and Information Engineering, Xi'an University of Post and Telecommunications, Xi'an, 710121, China (e-mail: xuezhemail@163.com)

Honggang Wang is with School of Communication and Information Engineering, Xi'an University of Post and Telecommunications, Xi'an, 710121, China (e-mail: whg_xian_cn@163.com)

Hanlu Zhang is with School of Communication and Information Engineering, Xi'an University of Post and Telecommunications, Xi'an, 710121, China (e-mail: roland_zhang@163.com)

Jinwei Song is with China Electronics Standardization Institute, Xi'an, 100007, China (e-mail: yunqimail@163.com)

Moreover, additional requirements are also necessary to facilitate stealth, which involves using minimum peak power to realize large detection range and ensuring easy accessibility in signal receiving and processing.

In recent years, radar waveform designing becomes a hotspot in radar research field [2-7], in which multicarrier radar owes its emergence to the prospering of multicarrier technology in communications. With respect to power consumption, Reference [8] took into account robust OFDM radar waveform design based on the philosophy of minimizing power consumption. Furthermore, in response to delay-Doppler radar applications, Reference [9] broadened OFDM waveform through embedding communication codes into OFDM chirp waveforms. Ultra-wideband OFDM radar has also been applied to earth observation and imaging [10,11]. In addition, the multi-input multi-output (MIMO) radar system [12] also referred to the technology developed for OFDM radar. In order to ensure convergence and coexisting of radio frequency (RF), Reference [13] designed a multicarrier radar-communications waveform.

The characteristics of multicarrier phase coded (MCPC) radar signal [14-15] are featured by introducing phase-coding to all carriers based on OFDM signals, to which certain advantages owe their emergence. The characteristics of multicarrier contribute to the advantage of MCPC signal with respect to expanded bandwidth by using narrow-band, easy operation and fast generation. In addition, the characteristics of phase-coding enables the profile of approximate ideal ambiguity function for MCPC radar signal, thereby ensuring its high resolution and outstanding anti-interference performance.

Reference [16] proposed a complementary block coding method to design a MCPC signal with low peak-to-mean envelope power ratio (PMEPR). Reference [17] designed a MCPC signal with low sidelobe power and PMEPR using Zad-off Chu phase sequence.

Although the above researches have designed multicarrier radar waveform from different perspectives, few articles focused on stealth radar waveform design using agility of multicarrier signal. In this study, we discussed designing an MCPC stealth radar waveform that is on the basis of chaotic phase modulation is discussed, upon which not only is the designed signal's ambiguity function analyzed, but also the method of signal pulse compression is studied.

II. Design of Multicarrier Chaotic Phase Coded Waveform

The mathematical expression for multicarrier chaotic phase coded signal [11] with carrier number N and phase modulated bits M is written as

$$f_{\mathrm{MCPC}}(t) = \sum_{n=0}^{N-1} \omega_n \sum_{m=0}^{M-1} a_{n,m} s(t - m t_{\mathrm{b}}) \exp(\mathrm{j}2\pi n \Delta f t), \qquad (1)$$

where $s(t) \equiv 1$ for $0 \le t < t_b$ and zero elsewhere, $a_{n,m} = e^{j\varphi_{n,m}}$ is the *m*-th element of the sequence modulating carrier *n*, $\varphi_{n,m}$ is the *m*-th phase element of the *n*-th sequence. $\omega_n = |\omega_n| e^{j\theta_n}$ denotes the complex weight corresponding to the *n*-th carrier, $|\omega_n|$ denotes the frequency weighted amplitude, θ_n is the frequency weighted phase being referred to as initial phase. Supposing that the frequency difference existing between neighboring two carriers Δf equals to the bit duration inverse t_b, we therefore obtain the OFDM.

For a conventional MCPC signal, its subcarrier encoding sequences usually involve Barker, P4 and Huffman codes, to which these commonly used encoding methods displays certain disadvantages in terms of encoding form and randomness.

In order to enhance the MCPC signal's agility and randomness, a chaotic sequence is adopted, of which is featured with high sensitivity to initial value, easy operability and identified reproducibility, thereby obtaining multicarrier chaotic phase-coded signal by introducing the quantum logistic map generated chaotic sequence [18-20] into phase modulation of the MCPC signal.

In this study, the aforementioned chaotic sequence being generated by quantum logistic mapping can be expressed as follows:

$$\begin{cases} f(k+1) \\ \quad = \mu\left[f(k) - |f(k)|^2 \right] - \mu p(k) \\ p(k+1) \\ \quad = -p(k)e^{-2\lambda} + e^{-\lambda}\mu \\ \times\left[\left(2 - f(k) - f^*(k)\right) p(k) - f(k)q^*(k) - f^*(k)q(k) \right] \\ q(k+1) \\ \quad = -q(k)e^{-2\lambda} + e^{-\lambda}\mu \\ \times\left[2\left(1 - f^*(k)\right) q(k) - 2 f(k) p(k) - f(k) \right] \end{cases} . \qquad (2)$$

In the above Equation (2), $\lambda \ge 6$ is the dissipative parameter, the adjustable parameter is $\mu \in (0,4)$. *f, p, q* represent complex numbers with f^* functioning as complex conjugate of *f* and as similarly of *q*. Here, the initial values are set to be real numbers, $f(0) \in (0,1)$, $p(0) \in (0,0.1)$, $q(0) \in (0,0.2)$, and then $f^* = f$, $q^* = q$. Accordingly, the quantum chaotic mapping possesses stronger randomness and higher aperiodicity.

The chaotic sequence generated by quantum logistic map is binarized as a set of MCPC signal chaotic phase modulation sequences, which is expected to have good autocorrelation performance. The maximum sidelobe value of correlation function being referred to as peak sidelobe level (PSLL) is adopted in evaluating autocorrelation performance of the chaotic sequences, to which smaller value indicates better performance, thereby further validating its higher independence and randomness.

Here, the iteration number (sequence length) that is composed of *N* steps begins from 1000 to 50000 with a unit step of 2000. Figure 1 is the diagram showing relationships in between the PSLL of sequence autocorrelation, iteration number and initial value of the binary quantum logistic chaotic sequence.

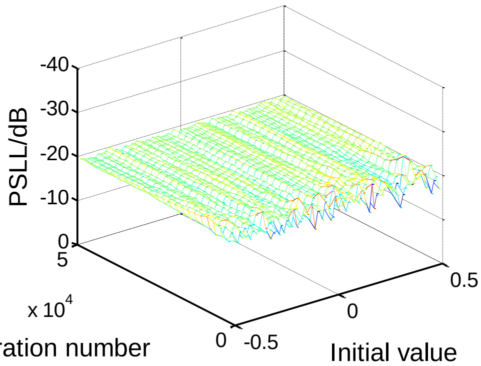

Fig. 1. Diagram showing relationships in between PSLL, iteration number and initial value.

As shown in the above figure, the autocorrelation performance of the binary quantum logistic chaotic sequences remains stable as the iteration number and initial value vary. The excellent autocorrelation performance still remains when the required long code length is not needed in practical applications.

The quantum logistic mapping is used to generate $L=M\times N$ chaotic biphase codes that can be expressed in the form of the set $\{c_1, c_2, c_3, \ldots c_L\}$. Using with Eq. (3), each carrier's phase in the MCPC signal can therefore be modulated. Hence, the multicarrier chaotic phase coded waveform based on binary quantum logistic mapping is obtained, which is denoted here as MCPC_QL,

$$\varphi_{n,m} = c_{M(n-1)+m} . \qquad (3)$$

Supposing that, $t = n t_b / N$, i.e., then *N* sampling points exist in a symbol duration. The length of the sampled MCPC_QL signal is *MN*.

By discretising the gate function $s(t)$, we obtain

$$s\left(\frac{t_{\mathrm{b}}}{N} n\right) = s(n) = R_N(n) = \begin{cases} 1, & 0 \le n \le N-1 \\ 0, & else \end{cases} . \qquad (4)$$

Therefore, $s(n t_{\mathrm{b}} / N - m t_{\mathrm{b}})$ can be written as $s(n - mN)$. The expression for the MCPC_QL sampling derived from Eq. (1) is

$$\begin{aligned} f(n) &= \sum_{k=0}^{N-1} \omega_k \sum_{m=0}^{M-1} a_{k,m} s(n - mN) \exp(\mathrm{j}\frac{2\pi}{N} kn) \\ &= \sum_{m=0}^{M-1} \left[\sum_{k=0}^{N-1} \omega_k a_{k,m} \exp(\mathrm{j}\frac{2\pi}{N} kn) \right] s(n - mN) \\ &= \sum_{k=0}^{N-1} \omega_k a_{k,0} \exp(\mathrm{j}\frac{2\pi}{N} kn) s(n) \\ &+ \sum_{k=0}^{N-1} \omega_k a_{k,1} \exp(\mathrm{j}\frac{2\pi}{N} kn) s(n-N) \\ &+ \cdots + \sum_{k=0}^{N-1} \omega_k a_{k,M-1} \exp(\mathrm{j}\frac{2\pi}{N} kn) s[n-(M-1)N] \\ &= \sum_{m=0}^{M-1} N \times \mathrm{IDFT}\left[\omega_k a_{k,m} \right] s(n - mN) \end{aligned} . \qquad (5)$$

So the MCPC_QL signal can be obtained by conducting inverse discrete Fourier transform (IDFT) with respect to the symbol matrix $[\omega_k a_{k,m}]_{N\times M}$ multiplied by *N*. Therefore, the generation of the MCPC_QL signal can be accomplished through conducting inverse fast Fourier transform (IFFT) operation to shorten the operation time. A flowchart showing the generation of the MCPC_QL signal using the IFFT is shown in Fig.2.

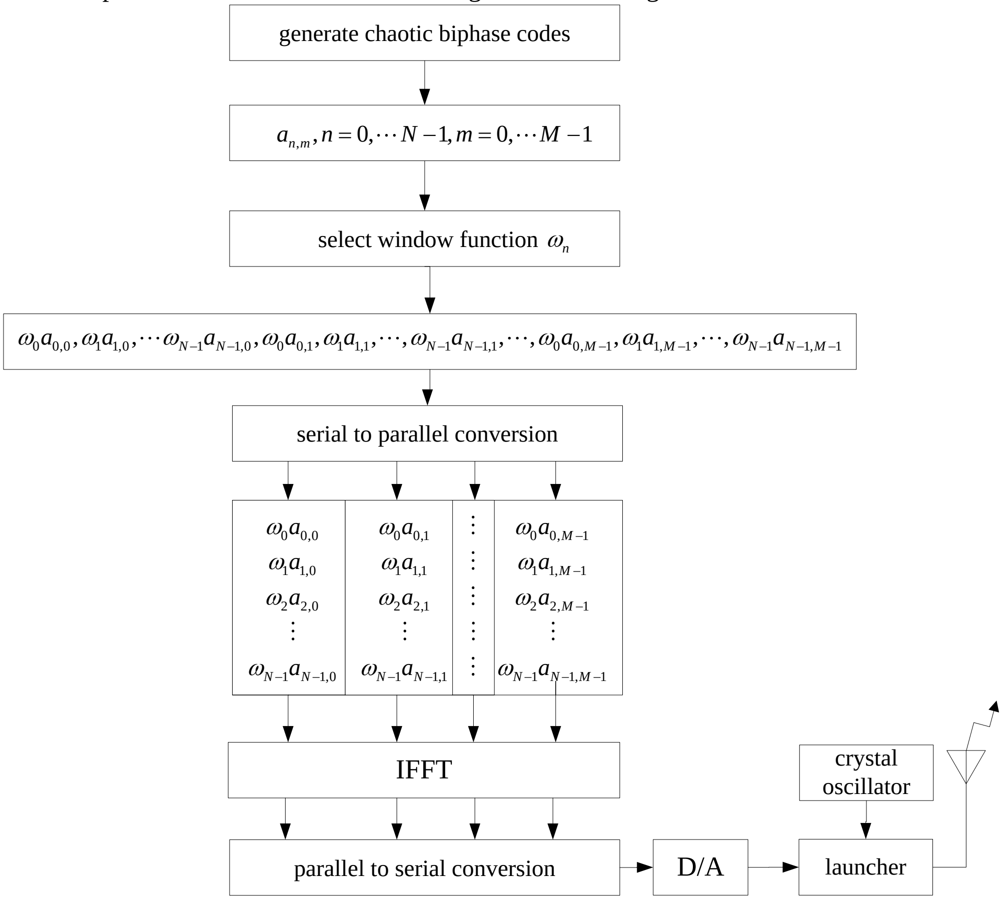

Fig. 2. Flowchart showing the generation of the MCPC_QL signal.

III. AMBIGUITY FUNCTION OF THE MCPC_QL

Following the principal of ambiguity function,

$$\chi(\tau,v)=\int_{-\infty}^{+\infty} f(t) f^*(t+\tau)\exp(\mathrm{j}2\pi vt)\mathrm{d}t . \quad (6)$$

Therefore, by substituting Eq. (1) into Eq. (6), it is obtained that

$$\begin{aligned}\chi(\tau,v)=&\int_{-\infty}^{+\infty}\sum_{n=0}^{N-1}\omega_n\sum_{m=0}^{M-1}a_{n,m}s(t-mt_\mathrm{b})\exp(\mathrm{j}2\pi n\Delta ft)\\&\times\sum_{n_1=0}^{N-1}\omega_{n_1}^*\sum_{m_1=0}^{M-1}a_{n_1,m_1}^*s^*(t+\tau-m_1t_\mathrm{b})\exp[-\mathrm{j}2\pi n_1\Delta f(t+\tau)]\exp(\mathrm{j}2\pi vt)\mathrm{d}t\\=&\sum_{n=0}^{N-1}\sum_{m=0}^{M-1}\sum_{n_1=0}^{N-1}\sum_{m_1=0}^{M-1}\omega_n\omega_{n_1}^*a_{n,m}a_{n_1,m_1}^*\exp(-\mathrm{j}2\pi n_1\Delta f\tau)\int_{-\infty}^{+\infty}\exp[\mathrm{j}2\pi(n-n_1)\Delta ft]\\&\times\exp(\mathrm{j}2\pi vt)s(t-mt_\mathrm{b})s^*(t+\tau-m_1t_\mathrm{b})\mathrm{d}t\end{aligned} . \quad (7)$$

Supposing that $(n-n_1)\Delta f+v=F_\mathrm{d}$, $\tau+(m-m_1)t_\mathrm{b}=t_\mathrm{s}$ and $t-mt_\mathrm{b}=t'$, Eq. (7) can therefore be simplified as

$$\begin{aligned}\chi(\tau,v)=&\sum_{n=0}^{N-1}\sum_{m=0}^{M-1}\sum_{n_1=0}^{N-1}\sum_{m_1=0}^{M-1}\omega_n\omega_{n_1}^*a_{n,m}a_{n_1,m_1}^*\exp(-\mathrm{j}2\pi n_1\Delta f\tau)\\&\times\exp(\mathrm{j}2\pi F_\mathrm{d}mt_\mathrm{b})\frac{\mathrm{e}^{\mathrm{j}\pi F_\mathrm{d}(t_\mathrm{b}-t_\mathrm{s})}\sin\left[\pi F_\mathrm{d}(t_\mathrm{b}-|t_\mathrm{s}|)\right]}{\pi F_\mathrm{d}},|\tau+(m-m_1)t_\mathrm{b}|<t_\mathrm{b}\\=&\chi_\mathrm{auto}(\tau,v)+\chi_\mathrm{cross}(\tau,(n-n_1)\Delta f+v),|\tau+(m-m_1)t_\mathrm{b}|<t_\mathrm{b}\end{aligned} , \quad (8)$$

where $\chi_\mathrm{auto}(\tau,v)$, which is called the auto-ambiguity function. This term is the result of $\chi(\tau,v)$ when the following conditions are satisfied: n=n_1, m=m_1, $F_\mathrm{d}=(n-n_1)\Delta f+v=v$, $t_\mathrm{s}=\tau$ and $|\tau+(m-m_1)t_\mathrm{b}|<t_\mathrm{b}\Rightarrow|\tau|<t_\mathrm{b}$

$$\begin{aligned}\chi_\mathrm{auto}(\tau,v)=&\sum_{\substack{n=0\\n=n_1}}^{N-1}\sum_{\substack{m=0\\m=m_1}}^{M-1}|\omega_n|^2|a_{n,m}|^2\exp(-\mathrm{j}2\pi n\tau\Delta f)\\&\times\exp(\mathrm{j}2\pi vmt_\mathrm{b})\frac{\mathrm{e}^{\mathrm{j}\pi v(t_\mathrm{b}-\tau)}\sin\left[\pi v(t_\mathrm{b}-|\tau|)\right]}{\pi v},|\tau|<t_\mathrm{b}\end{aligned} . \quad (9)$$

$\because a_{n,m}=\mathrm{e}^{\mathrm{j}\varphi_{n,m}}$ $\therefore |a_{n,m}|^2=1$, when $|w_n|^2=1$, Eq. (9) can be simplified as

$$\begin{aligned}\chi_\mathrm{auto}(\tau,v)=&\frac{\mathrm{e}^{\mathrm{j}\pi v(t_\mathrm{b}-\tau)}\sin\left[\pi v(t_\mathrm{b}-|\tau|)\right]}{\pi v}\\&\times\sum_{\substack{n=0\\n=n_1}}^{N-1}\exp(-j2\pi n\tau\Delta f)\sum_{\substack{m=0\\m=m_1}}^{M-1}\exp(j2\pi vmt_\mathrm{b}),|\tau|<t_\mathrm{b}\\=&\frac{\mathrm{e}^{j\pi v(t_\mathrm{b}-\tau)}\sin\left[\pi v(t_\mathrm{b}-|\tau|)\right]}{\pi v}\\&\times\frac{1-\exp(\mathrm{j}2\pi vMt_\mathrm{b})}{1-\exp(\mathrm{j}2\pi vt_\mathrm{b})}\sum_{\substack{n=0\\n=n_1}}^{N-1}\exp(-\mathrm{j}2\pi n\tau\Delta f)\\=&\frac{\mathrm{e}^{\mathrm{j}\pi v(t_\mathrm{b}-\tau)}\sin\left[\pi v(t_\mathrm{b}-|\tau|)\right]}{\pi v}\\&\times\frac{1-\exp(\mathrm{j}2\pi vMt_\mathrm{b})}{1-\exp(\mathrm{j}2\pi vt_\mathrm{b})}\frac{1-\exp(-\mathrm{j}2\pi\tau\Delta fN)}{1-\exp(-\mathrm{j}2\pi\tau\Delta f)},|\tau|<t_\mathrm{b}\end{aligned} . \quad (10)$$

When $n\neq n_1$ and $m\neq m_1$, it can be obtained that $\chi_\mathrm{cross}(\tau,(n-n_1)\Delta f+v)$, which is called the cross-ambiguity function:

$$\begin{aligned}&\chi_{\rm cross}(\tau,(n-n_1)\Delta f+v)\\&=\sum_{\substack{n=0\\n\neq n_1}}^{N-1}\sum_{\substack{m=0\\m\neq m_1}}^{M-1}\sum_{n_1=0}^{N-1}\sum_{m_1=0}^{M-1}\omega_n\omega_{n_1}^{*}a_{n,m}a_{n_1,m_1}^{*}\exp(-{\rm j}2\pi n_1\Delta f\tau)\\&\times\exp({\rm j}2\pi F_{\rm d}mt_{\rm b})\frac{{\rm e}^{{\rm j}\pi F_{\rm d}(t_{\rm b}-t_{\rm s})}\sin\left[\pi F_{\rm d}(t_{\rm b}-|t_{\rm s}|)\right]}{\pi F_{\rm d}},\\&\left|\tau+(m-m_1)t_{\rm b}\right|<t_{\rm b}\end{aligned}\quad(11)$$

where $\chi_{\rm cross}(\tau,(n-n_1)\Delta f+v)$ has little influence on $\chi(\tau,v)$.

Supposing that N=M=13, t_b=10^{-6}, the corresponding ambiguity function of the MCPC_QL is therefore illustrated in Fig. 3. Figure 4 depicts the ambiguity function of the MCPC signal based on P4 code. As shown in Figures 3 and 4, the ambiguity function of the MCPC_QL signal exhibits a thumbtack profile, displaying its high range and speed resolution, whereas the ambiguity function of the MCPC_P4 exhibits higher autocorrelation sidelobes and large fluctuations in the Doppler axis, posing detrimental impacts on measuring speed and distance.

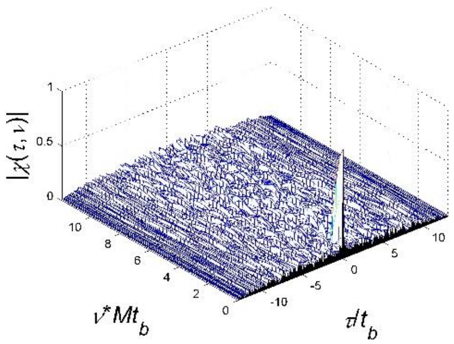

Fig. 3. Ambiguity function of the MCPC_QL.

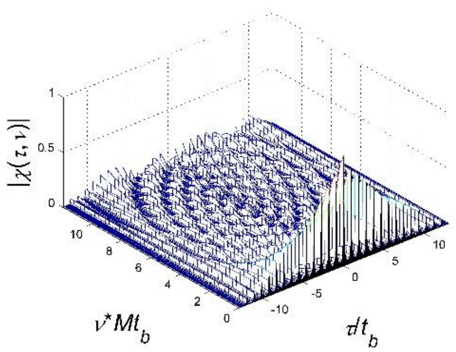

Fig. 4. Ambiguity function of the MCPC_P4.

The autocorrelation function's PSLL of the MCPC_QL varies with the carrier number N, and the symbol number M ranging from 3 to 51 with a step size of 2 is shown in Fig. 5, which means smaller N and M indicate degradation in the autocorrelation performance.

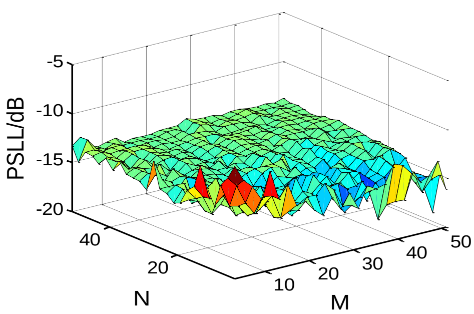

Fig. 5. Impact imposed by carrier number N and symbol number M on autocorrelation's PSLL of MCPC_QL

The PSLL's value decreases as the values of N and M increase, and that the fluctuation of the PSLL curve tends to be stable.

IV. Pulse Compression of the MCPC_QL Signal

Being one of the most critical procedures in radar signal processing [21], pulse compression, upon which subsequent missions are depended, balances the detection ability of a radar with its distance resolution. In this study, through utilizing the multicarrier characteristics of the MCPC_QL signal, operations of pulse compression can be performed on corresponding signals adopting the FFT method. The impulse response of the matched filtering of the MCPC_QL signal $f(t)$ is

$$h(t)=f^{*}(Mt_{\rm b}-t).\quad(12)$$

The sampling rate is

$$f_s=LN\Delta f=LN/t_{\rm b},\quad(13)$$

where L>1, meaning that each symbol sample of LN points can effectively avoid compression losses. After sampling the signal $f(t)$, the sampled signal $f(k)$ is therefore obtained:

$$f(k)=\sum_{n=1}^{N}\sum_{m=1}^{M}w_na_{n,m}s\left[\frac{kt_{\rm b}}{LN}-(m-1)t_{\rm b}\right]\exp({\rm j}2\pi(n-1)\frac{k}{LN}).\quad(14)$$

The $h(t)$ is sampled with the same sampling rate

$$h(k)=h(t)|_{t=kT}=f_1^{*}(Mt_{\rm b}-\frac{kt_{\rm b}}{LN}).\quad(15)$$

The output of the matched filter is

$$y(k)=\sum_{i=-\infty}^{\infty}f(i)h(k-i).\quad(16)$$

By substituting $f(k)$ and $h(k)$ into Eq. (16), it can be obtained that

$$\begin{aligned}y(k)&=\sum_{i=-\infty}^{\infty}\sum_{n=0}^{N-1}\sum_{m=0}^{M-1}\omega_na_{n,m}s\left(\frac{it_{\rm b}}{LN}-mt_{\rm b}\right)\exp\left({\rm j}2\pi n\frac{i}{LN}\right)\\&\times\sum_{n_1=0}^{N-1}\sum_{m_1=0}^{M-1}\omega_{n_1}^{*}a_{n_1,m_1}^{*}s^{*}\left[Mt_{\rm b}-\frac{(k-i)t_{\rm b}}{LN}-m_1t_{\rm b}\right]\exp\left[-{\rm j}2\pi n_1(M-\frac{k-i}{LN})\right]\\&=\sum_{n=0}^{N-1}\sum_{m=0}^{M-1}\sum_{n_1=0}^{N-1}\sum_{m_1=0}^{M-1}\omega_n\omega_{n_1}^{*}a_{n,m}a_{n_1,m_1}^{*}\exp\left(-{\rm j}2\pi n_1M\right)\exp\left({\rm j}2\pi n_1\frac{k}{LN}\right)\\&\times\sum_{i=-\infty}^{\infty}\exp\left(-{\rm j}2\pi(n_1-n)\frac{i}{LN}\right)s\left(\frac{it_{\rm b}}{LN}-mt_{\rm b}\right)s^{*}\left[Mt_{\rm b}-\frac{(k-i)t_{\rm b}}{LN}-m_1t_{\rm b}\right]\end{aligned}.\quad(17)$$

Supposing that $\frac{it_{\rm b}}{LN}-mt_{\rm b}=i'$, Eq. (17) can be simplified as

$$\begin{aligned}y(k)&=\sum_{n=0}^{N-1}\sum_{m=0}^{M-1}\sum_{n_1=0}^{N-1}\sum_{m_1=0}^{M-1}\omega_n\omega_{n_1}^{*}a_{n,m}a_{n_1,m_1}^{*}\exp\left(-{\rm j}2\pi n_1M\right)\\&\times\exp\left({\rm j}2\pi n_1\frac{k}{LN}\right)\exp\left[-{\rm j}2\pi(n_1-n)m\right]\\&\times\sum_{i'=-\infty}^{\infty}\exp\left(-{\rm j}2\pi\frac{(n_1-n)}{t_{\rm b}}i'\right)s(i')\\&\times s^{*}\left[i'+Mt_{\rm b}+(m-m_1)t_{\rm b}-\frac{kt_{\rm b}}{LN}\right]\end{aligned}.\quad(18)$$

Supposing that $Mt_{\rm b}+(m-m_1)t_{\rm b}-\frac{kt_{\rm b}}{LN}=i_s$, $\frac{(n_1-n)}{t_{\rm b}}=F_{\rm B}$, the final summation of Eq.(18) is

$$\begin{aligned}&\sum_{i=-\infty}^{\infty}\exp\left(-{\rm j}2\pi F_{\rm B}i\right)s(i)s^{*}\left(i+i_s\right)\\&=\exp\left[-{\rm j}\pi F_{\rm B}(LN-i_s)\right]\frac{\sin[\pi F_{\rm B}(LN+1-|i_s|)]}{\sin(\pi F_{\rm B})}\end{aligned}.\quad(19)$$

Therefore, the output of pulse compression can be expressed by Eq. (20). It can be seen from the generation of the MCPC_QL signal shown in Fig. 2 that the signal is substantially the discrete Fourier transform (DFT) of the symbol matrix $[\omega_n a_{n,m}]_{N\times M}$ by columns:

$$\begin{aligned} y(k) &= \sum_{n=0}^{N-1}\sum_{m=0}^{M-1}\sum_{n_1=0}^{N-1}\sum_{m_1=0}^{M-1}\omega_n\omega_{n_1}^{*}a_{n,m}a_{n_1,m_1}^{*}\exp\left(-\mathrm{j}2\pi n_1 M\right) \\ &\times\exp\left(\mathrm{j}2\pi n_1\frac{k}{LN}\right)\exp\left[-\mathrm{j}2\pi(n_1-n)m\right] \qquad . \qquad (20) \\ &\times\exp\left[-\mathrm{j}\pi F_{\mathrm{B}}(LN-i_s)\right]\frac{\sin[\pi F_{\mathrm{B}}(LN+1-|i_s|)]}{\sin(\pi F_{\mathrm{B}})}, \\ &\left|Mt_b+(m-m_1)t_{\mathrm{b}}-\frac{kt_{\mathrm{b}}}{LN}\right|<LN \end{aligned}$$

Therefore, the DFT can be used to calculate the symbol matrix in a sliding way, and then it can be correlated with the conjugate of the encoding sequence to get the pulse pressure output. Fig. 6 demonstrates a DFT-based diagram of pulse compression of the MCPC_QL (N=M=7 is taken as an example).

In the above figure, i is the count variable with an initial value of 1. The sampling rate is set as $LN\Delta f$, where L>1, and the LN points are sampled in the symbol. Due to the M symbols involved in the MCPC_QL signal, LMN points therefore exist. Hence, $f_d(n)$ is set as the expression of the MCPC_QL signal after being sampled. The method of pulse compression on the MCPC_QL signal based on the DFT is described as follows.

Step 1. LMN-1zeros are added at the tail of $f_d(n)$.
Step 2. $f_d(i)$ is set as the starting point, and data with length of LMN are divided into M segments with length of LN.
Step 3. Data of M points for each LN path are obtained by serial to parallel conversion.
Step 4. LN point FFT by columns is conducted on the parallel data M times. The first N points from the FFT result are taken to form N×M parallel data with N paths and M points for each path.
Step 5. N×M parallel data are correlated with the phase encoding of the MCPC_QL.
Step 6. The results of Step5 is added to get the i-th output of pulse compression.
Step 7. i=i+1. If $i\leqslant LMN$, return to Step2 and repeat until i>LMN.

Taking the MCPC_QL signal with N=M=7 as an example, the results of pulse compression based on the FFT and on conventional matched filtering methods are shown in Fig. 7, to which the result of FFT-based pulse compression is similar to that of the conventional matched filtering method. However, the calculation speed of the FFT-based pulse compression is therefore improved, to which the adopting of the FFT method can be primarily attributed.

Throughout the pulse compression process performed on MCPC_QL signal using the FFT method, the symbols of each carrier and of each code element $[\omega_n a_{n,m}]_{N\times M}$ are therefore obtained, by which each carrier can be recovered, displaying the real part after performing pulse compression on each carrier of the signal as shown in Fig. 8. The result of the MCPC_QL pulse compression based on the FFT (the real part is not normalized) is shown in Fig .9.

As can be seen from Fig.8, the spiky profile of each carrier occurs in same positions due to its equal pulse widths. The pulse pressure spikes of each carrier appear at the same position, and the resultant pulse compression output (Fig. 9) is the N (number of carriers) multiples of the pulse compression result of each carrier.

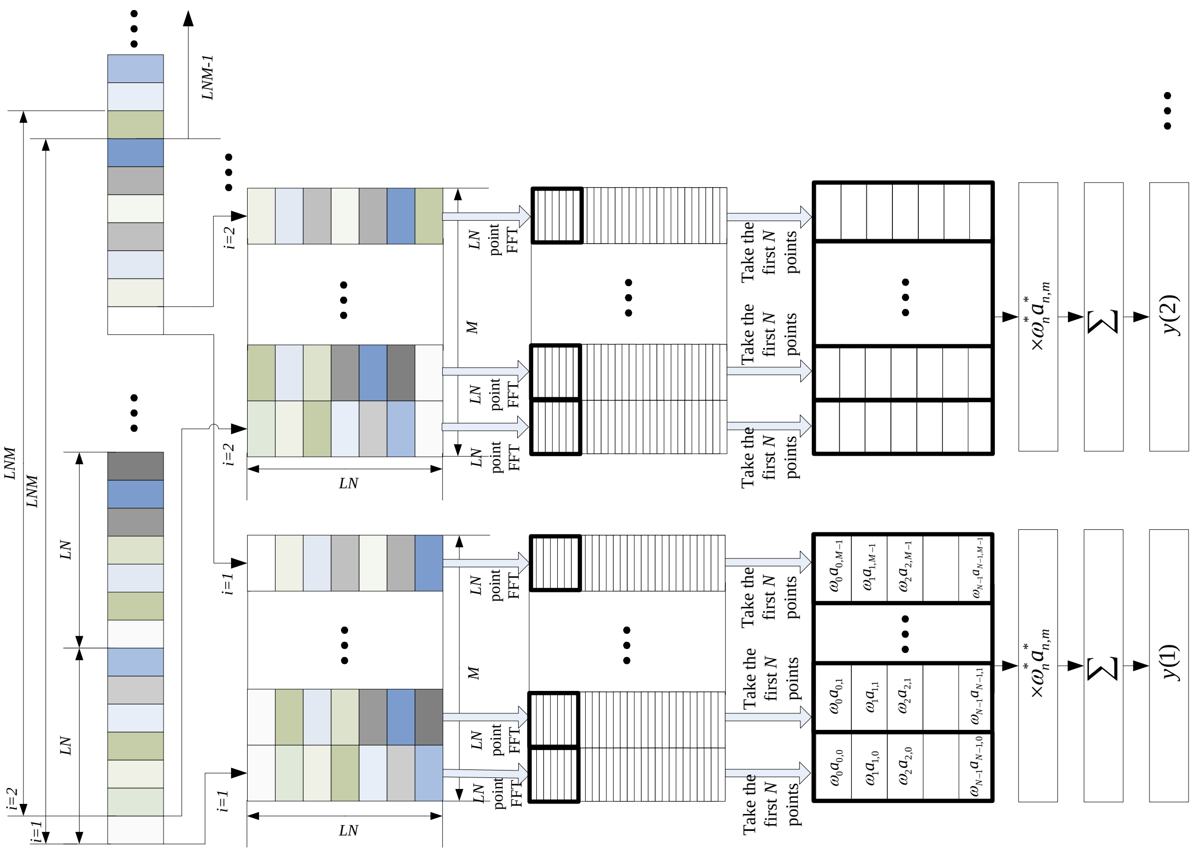

Fig. 6. Pulse compression of the MCPC_QL based on the DFT.

In specific, with respect to each subcarrier, the sidelobe fluctuations of each subcarrier's pulse compression result differ, to which adding these fluctuations together will cause either profile superposition or profile cancellation in sidelobe of pulse compression result. Consequently, the superposition leads to the sidelobe base elevating while the cancellation results in the sidelobe base lowering, thus further making the final pulse compression result being featured not only with its mainlobe exhibiting spiky profile but also with small fluctuating profile under low base of the sidelobe.

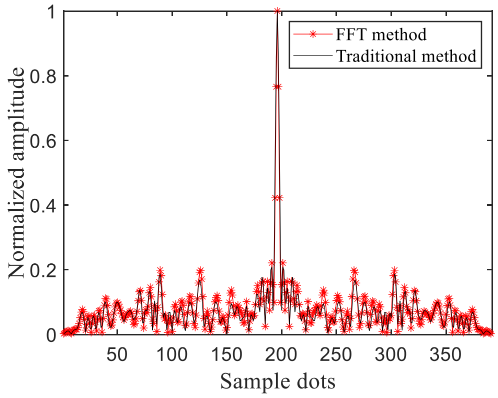

Fig. 7. Comparison of the two pulse compression methods

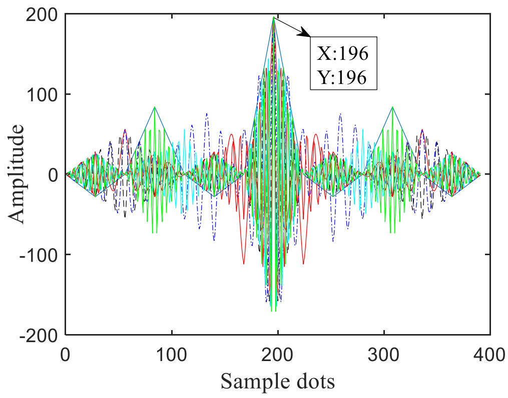

Fig. 8. Subcarrier pulse compression result

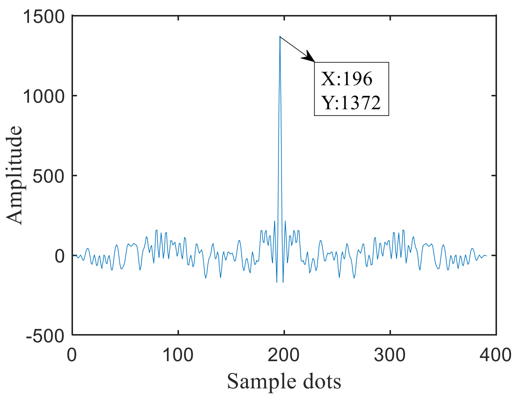

Fig. 9. Pulse compression result of the the MCPC_QL signal

V. Conclusion

In this paper, a larger bandwidth was generated by the proposed designing of the MCPC_QL radar signal, thereby ensuring higher distance resolution. The orthogonal subcarrier structure of the designed signal not only ensures small interference in between the carrier frequencies, but also facilitates full utilization of the frequency band. The introducing of chaotic phase modulation features the waveform with lots of characteristics in terms of code agility, randomness, waveform diversity, and of a thumbtack ambiguity function, further enabling the designed waveform to meet the requirements of a stealth radar waveform.

Despite the aforementioned research findings, certain factors are not taken into account in this paper, which may potentially impose advantageous effects or disadvantageous encumbrance on the performance of the stealth radar waveforms. For instance, the adaptability of radar waveform to environment is not considered. In order to lay solid theoretical foundations for designing stealth radar waveforms, our future research interest will be focusing on the above factor, paving way for implementing the proposed radar waveforms in practical applications of intelligent adaptive design.

References

[1] Lynch, D, "*Introduction to RF Stealth*". Translated by Yufang Shen, Northwestern Polytechnical Uniersity Press, Xi'an, China, 2009.

[2] Ravi Kishore T and Deergha Rao K, "Automatic Intrapulse Modulation Classification of Advanced LPI Radar Waveforms," *IEEE Transactions on Aerospace & Electronic Systems*., vol. 53, no. 2, pp. 901-914, 2010.

[3] Chenguang Shi, Fei Wang, Sana Salous and Jianjiang Zhou, "Low Probability of Intercept-Based Radar Waveform Design for Spectral Coexistence of Distributed Multiple-Radar and Wireless Communication Systems in Clutter," *Entropy*., vol. 20, no. 3, pp.197, 2018.

[4] Levanon, N., Mozeson, E, "*Radar signals*". John Wiley & Sons, New York, 2004.

[5] Yu Yao, Junhui Zhao and Lenan Wu, "Cognitive Design of Radar Waveform and the Receive Filter for Multitarget Parameter Estimation," *Journal of Optimization Theory and Applications*., vol.181, no. 2, pp.684-705, 2019.

[6] Tianduo Hao, Chen Cui, Yang Gong and Yuncheng Li, "Efficient low-PAR radar waveform design method based on the alternating direction method of multipliers for multiple missions," *IET Radar Sonar Navig*., vol. 13, no. 3, pp. 392-401, 2019.

[7] Yuanpin Cheng, Don Brutzman, Phillip E.Pace and Arnold H.Buss, "Hybrid High-Fidelity Modeling of Radar Scenarios using Atemporal, Discrete Event, and Time-Step Simulation," Lecture Notes in Engineering and Computer Science: Proceedings of The World Congress on Engineering and Computer Science 2016, WCECS 2016, 19-21 October, 2016, San Francisco, USA, pp764-770.

[8] Chenguang Shi, Fei Wang, Mathini Sellathurai and Jianjiang Zhou, "Power minimization-based robust OFDM radar waveform design for radar and communication systems in coexistence," *IEEE Transactions on Signal Processing*., vol. 66, no. 5, pp.1316-1330, 2017.

[9] Mengjiao Li, Wenqin Wang and Zhi Zheng, "Communication-embedded OFDM chirp waveform for delay-Doppler radar," *IET Radar Sonar and Navigation*., vol.12, no. 3, pp. 353-360, 2018.

[10] HaitaoWang, Junpeng Yu, Wenzhen Yu and De Ben, "Adaptive waveform design for distributed OFDM MIMO radar system in multi-target scenario," *Chinese Journal of Aeronautics*., vol.31, no.3, pp. 567-574, 2018.

[11] Xinhai Wang, Gong Zhang, Fangqing Wen and De Ben, "Schemes for synthesizing high-resolution range profile with extended OFDM-MIMO," *Journal of Systems Engineering & Electronics*., vol.28, no.3, pp.424-434, 2017.

[12] Hui Li, Yongbo Zhao, Zengfei Cheng and Dazheng Feng, "OFDM Chirp Waveform Diversity Design With Correlation Interference Suppression for MIMO Radar," *IEEE Geoscience & Remote Sensing Letters*., vol.14, no.7, pp.1032-1036, 2017.

[13] Marian and Visa, "Multicarrier radar-communications waveform design for RF convergence and coexistence," *IEEE International Conference on Acoustics, Speech and Signal Processing*, Brighton, UK, May 2019, pp. 7780-7784.

[14] Levanon N, "Multifrequency complementary phase-coded radar signal," *IET Radar Sonar and Navigation.*, vol.147, no.6, pp. 276-284, 2000.

[15] Wang Jiegui and Zhang Pengcheng, "Jamming technique of MCPC modulation repeater against phase-coded stepped-frequency radar," (in Chinese), *Acta Electronica Sinica*., vol.45, no.01, pp.89-97, 2017.

[16] C.G.Raghavedra, B.R.Prajwal, G.B.Druva, R.Keerthana, S.Meghna and N.N.S.S.R.K.Raghavendra, "Reduction of envelope fluctuations in OFDM radar signal using coding technique," *International conference on communication and signal processing*, Chennai, India, April, 2018, pp. 802-805.

[17] Raghavedra C.G, Harsha N and Prasad Nnssrk, "Sidelobe reduction of multicarrier radar signals using Zad-off Chu polyphase sequence," *Proceedings of the International Conference on Inventive Research in Computing Applications*, Coimbatore, India, July 2018, pp. 1057-1061.

[18] A. Akhshani, A.Akhavan, S.-C. Lim, Z.Hassan, "An image encryption scheme based on quantum logistic map," *Communications in Nonlinear Science & Numerical Simulation*., vol.17, no.12, pp. 4653-4661, 2012.

[19] Yukai Tong, Changlong Zhu, Xueqian Wang and Jing Zhang, "Controlling chaos in superconducting quantum interference devices," *Proceedings of the 36th Chinese control conference*, Dalian, China, July 2017, pp. 1012–1015.

[20] Bowen Chen, Jiang Lei, Xiaowen Liu and Qun, Zhang, "Ultra-wideband signal detection based on chaotic quantum particle swarm optimization FHN model method," *9th IEEE International conference on communication software and networks*, Guangzhou, China, May 2017, pp. 901–905.

[21] N.Balaji, M.Srinivasa rao, K.Subba Rao, S.P. Singh and N. Madhusudhana Reddy, "FPGA implementation of the ternary pulse compression sequences, " Lecture Notes in Engineering and Computer Science: Proceedings of The International MultiConference of Engineers and Computer Scientists 2008, IMECS 2008, 19-21 March, 2008, Hong Kong, pp231-235.